TRUE ORTHOPHOTO CREATION THROUGH FUSION OF LIDAR DERIVED DIGITAL SURFACE MODEL AND AERIAL PHOTOS

A. Kato [a, *], L. M. Moskal[b], P. Schiess[b], D. Calhoun[c], M. E. Swanson[d]

[a] Graduate School of Horticulture, Chiba University, 648 Matsudo Matsudo-shi Chiba 2718510 Japan
akiran@faculty.chiba-u.jp
[b] Precision Forestry Cooperative, School of Forestry, College of Environment, University of Washington, Box 352100 Seattle, WA 98195-2100 USA
(lmmoskal, schiess)@u.washington.edu
[c] Laboratoire d'Etudes des Transferts et de Mecanique des Fluides, Commissariat l'Energie Atomique F-91191 Gif-sur-Yvette Cedex, France
donna.calhoun@cea.fr
[d] Department of Natural Resource Sciences, Washington State University 177 Johnson Hall Pullman, WA 99164-6410 USA
markswanson@wsu.edu

KEY WORDS: Digital, LIDAR, Fusion, Orthorectification, Orthoimage

ABSTRACT:

Data fusion between aerial photos and LiDAR provides better estimates in forestry and ecological applications, because LiDAR mainly provides the structural information of objects and aerial photo can add spectral information to them. Without the data fusion, an accurate identification of tree crown information from two dimensional data is difficult due to shaded and shadow pixels cast on the image and image distortion. The aerial photogrammetric techniques cannot reconstruct the objects accurately in three dimensional spaces if they are not clearly visible on the photos. The conventional orthophotos, therefore, still have image distortion due to an inappropriate Digital Surface Model (DSM). LiDAR provides a more suitable surface of tree crown structure in three-dimensional spaces. This LiDAR-derived DSM could be used in conjunction with conventional photogrammetric techniques to rectify aerial photos and produce true orthophotos for each image. The existence of different perspective points from the use of multiple images results in different illumination and shadows cast on the DSM from the angle between the sun and the camera. In previous studies, a Z-buffer algorithm was applied for the occlusion detection and compensation. However, the technique was computationally intensive. In this study, the camera view and sun-oriented hillshade were generated using the LiDAR-derived DSM. The hillshade surfaces distinguished between the exposed and the occluded side of the DSM during the composition process of respective true orthophotos. This technique constituted a simpler approach and is applicable to data fusion between LiDAR and multispectral imagery to make an orthographically rectified image.

1. INTRODUCTION

1.1 Data Fusion

Data fusion data derived from different remote sensing sensors has been used for numerous applications. The improvement of detecting objects was demonstrated by data fusion among several different sensors to derive better results than that derived by each sensor solely. There are limits in two dimensional image analyses for forestry application. Those issues and the advantage of data fusion are discussed in the following subsection.

1.2 The limitation of two-dimensional image analysis

The limits of two dimensional image data have been addressed with several crown delineation techniques such as image processing algorithm (Brandtberg and Walter, 1998; Erikson, 2003), local maximum filter with semivariogram (Wulder et al., 2000), and valley following algorithms (Gougeon, 1995; Leckie et al, 2003, 2005). Brandtberg and Walter (1998) processed a near-infrared image to delineate tree crowns. They detected crown edges on the image for crown segmentation. The accuracy was 70% compared with manual delineation. Such delineation only worked for the visible portion of tree crowns because of the light illumination. Natural forests canopies are comprised of tree crowns with various sizes and shapes and complex vertical tree composition. This presents a challenge for crown delineation based on two-dimensional data. Leckie et al. (2005) found several other important issues in two-dimensional image analysis: different sun angles among multi-year data, different sensor view angles, and similar spectral signatures of trees within the old growth stand. The various shade and shadowing effects caused different delineation results. The sensor view angle, therefore, should be considered for further improvement of crown delineation technique.

1.3 Advantage of data fusion

For the conventional photogrammetric technique, creating automated Digital Surface Model (DSM) over a dense forest is prone to error because of the difficulty of matching pixels in the tree canopy between two stereo photos taken at different viewing angles. Light Detection and Ranging (LiDAR) is, therefore, a good alternative tool to create better DSMs to rectify the aerial images. The LiDAR derived Canopy Height Model (CHM) was used for the valley following algorithm to compare with the results from digital aerial photos (Leckie et al., 2003). They found that digital aerial photos were better for the delineation of tree crowns; while the LiDAR derived CHM was

* Corresponding author

better for open canopy areas. The LiDAR derived CHM was better suited in clearly distinct area among neighbouring pixels between trees and shrub (or ground). LiDAR was well suited to measure tree height and large tree crown delineation (Leckie et al., 2003). For the data fusion between aerial photos and LiDAR, a simply approach can be taken to form a direct link between LiDAR and orthophoto plainmatric coordinate. The orthophoto still has, however, distorted objects because of the insufficient quality of DTMs or DSMs that are generally used to rectify the images. Therefore, the color values assigned on an orthophoto does not generally match with the LiDAR coordinates. The orthophoto creation should be improved by better data fusion approaches.

As the better applications of data fusion between the LiDAR derived high resolution data and aerial photos, St-Onge et al (2004) used LiDAR derived Digital Terrain Model (DTM) to measure tree height using stereo pair of aerial photos. Their approach can be useful for the change detection of tree height over time when historical photos are applied for comparison. Rönnholm et al. (2004) used the backprojection approach with exterior orientation parameters derived by aerial triangulation process from stereo pair of aerial photos. They draped LiDAR points on terrestrial digital images. Their approach explicitly showed which part of tree crown the LiDAR points were reflected from and was used for calibration in LiDAR acquisition accuracy.

1.4 True orthophoto generation

A 'true' orthophoto has been created for detecting buildings in the urban area (Amhar et al., 1998, Habib et al., 2007, Rau et al., 2002, Schickler and Thorpe, 1998, Zhou et al., 2005) and forested area (Sheng et al., 2003). Ambar et al. (1998) defined "true orthophoto" as an orthophoto that is rectified orthographically. The true orthophoto, therefore, does not have any image distortion of objects on the final image. Ideally it rectifies the structure of trees in an upright position on the image. Ambar et al. used Digital Building Models (DBMs) to find the visible side of building from the photo projection center using Z-buffer algorithm. The Z-buffer algorithm is also called hidden surface removal in computer graphics (Angel, 2003) and determines the visibility of the objects on the photos. In transformation of ground coordinate to image space coordinate, the corresponding location between them is a many-to-one relationship (Sheng et al., 2003). The Z-buffer algorithm uses the distance from the photo projection center and determines the closest object to the projection center and occludes all others. In this way, the ground coordinates of the visible sides of objects are only selected and matched with the corresponding pixel on the photo. Furthermore, it was reported that the false occlusion was found using the direct method of Z-buffer algorithm, if the sampling distance on the image was less than the DSM resolution (Amhar et al., 1998, Habib et al., 2007, Rau et al., 2002). Habib et al. (2007) showed that false occlusion caused the black grid lines in the ground coordinate as an example when the sampling distance did not match between the image space and the ground coordinate. Habib er al. (2007) also used radial and spiral sweep methods to resolve the issue of the false occlusion without DBMs in urban area. The occluded area of a master image was filled with images from a slave image (Rau et al., 2002). In other words, orthophotos created from different camera view angles were used to compensate the occluded area to produce a gapless composite image (Sheng et al,, 2003). When the finer resolution true orthophotos were merged into a larger one, occluded areas were filled in by the color values derived from orthophotos using an angle-based photo composition scheme (Sheng et al., 2003), seam line adjustment (Schickler and Thorpe, 1998), and histogram matching (Rau et al., 2002, Zhou et al., 2005). These methods were complicated, because the color values from different perspective photos were variable and not well calibrated. There was a photographic "light fall-off effect" which creates the darker colors at the edge (Sheng et al., 2003). A relatively simpler approach using the hillshade function is, therefore, introduced in a large area for occlusion detection and compensation in this study.

1.5 Hillshade method for occlusion detection and compensation

Hillshade surface utilized by ArcGIS (ESRI Inc.) has been used for surface temperature change analysis (Hais and Kučera, 2008), making moisture index in landscape (Iverson et al., 1997), the visual investigation of landslide area (Van Den Eeckhaut et al., 2005, 2007), identifying tectonic phase (Pellegrini et al., 2003), and urban growth modeling (Mahiny and Gholamalifard, 2007). The hillshade function has been mainly used for landscape analysis and has not been used for true orthophoto generation. For forestry application, Kane et al. (2008) used the hillshade function for self-shadowing effect to characterize the stand condition. They cast the shadow artificially on the forested landscape using LiDAR derived CHM.

The advantage of this function is to distinguish which side of a surface is visible to the light source. The light source can be the sun or camera location. The parallel rays from the sun were used for hillshade when the shadow is cast onto the surface, because the distance of the sun is virtually infinite. But the camera location mounted on airborne vehicle is in lower altitude and this function was, therefore, customized to have radial arrays from camera location to cast the shadow on the surface (a central projection).

2. OBJECTIVES

In order to compose a LiDAR rectified image that is displacement free, this paper used photogrammetric relationships to assign color values from original perspective image directly to the LiDAR derived DSM (the backprojection process was used). The assigned color was mapped onto its LiDAR plainmatric coordinates in two dimensions to make a true orthophoto from each perspective image. At the final stage of the process, the light reflectance between camera view and sun angle was considered using hillshade function. The shadowing effect of hillshade surface, therefore, was used for occlusion detection and compensation during the composition process. The main discussion points of this paper are:

1) accuracy of aerial triangulation* and backprojection process.
2) occlusion detection and compensation using sun and camera view hillshade.

* aerial triangulation in this study is achieved by using the Leica Photogrammetric Suite (LPS, Leica Geosystems, Inc.).

In this paper, a LiDAR derived DSM is used to rectify each original perspective photo to make a true orthophoto. To make a gapless composite image, the occluded areas are detected using values of hillshade function.

3. DATA

The research area is located in the Washington State Park Arboretum at the south end of the University of Washington and east of downtown Seattle, WA. The total area is 0.93 km^2. The terrain of this study area is moderate in slope, and the site is in a relatively urban setting. Arboretum is in the city so that building and other distinctive objects are readily available for Ground Control Points (GCPs) over the site for the aerial triangulation process for the data fusion technique.

Aerial photos show an electromagnetic reflectance of solar radiation. The reflectance depends on the angle between sun and the projection center of each photo relative to the objects on and above the ground. These reflectance values are not calibrated like multispectral images. Each aerial photo collects one central projected perspective view. The camera settings used in this study are shown in Table 1. Three consecutive aerial photos (named Image1, Image2, and Image3 from the South) along the flight line are used with 60% overlap (endlap) between photos from south to north of the Arboretum. Note that the capture dates of the photos and LiDAR were different. The year was, however, the same. The solar horizontal and vertical angle are calculated by their timestamp using a solar position calculator provided by NOAA (National Oceanic and Atmospheric Administration) Surface Radiation Research Branch.

Airborne LiDAR data was acquired in the same coverage area of aerial photos at the same year. LiDAR sensor setting is shown in Table 2. Aerial photo was taken during leaf-on season and LiDAR was acquired during leaf-off season. Stands of this study area are heterogeneous, multi-aged mixtures of coniferous and deciduous tree species. The seasonal error can by caused over the deciduous tree area.

Camera of aerial photos	
Date of acquisition	July 26th, 2005
Camera type	Jena LMK 2021
Average flying height	~2531 m
Focal length	210.914 mm
Scan Resolution	15 cm (photo scale was 1:12,000)

Table 2. Airborne LiDAR sensor setting

LiDAR sensor setting	
Acquisition data	March 17th, 2005
Laser sensor	Optec ALTM 3100
Laser wavelength	1064 nm (Near-infrared red)
Laser point densisty range	3 to 20 points/m^2

Table 1. Camera settings of aerial photos

4. METHODOLOGY

4.1 Aerial triangulation process

Stereo photos were used to rectify the image to make orthophotos using a series of control and tie points. The aerial triangulation process depends upon known exterior orientation parameters determined by the relationship between image coordinates and known ground coordinates. These parameters determine the orientation of each aerial photo and the location of the perspective point (camera location). The aerial photos were triangulated using Leica Photogrammetric Suite (LPS, Leica Geosystems, Inc.).

4.2 LiDAR derived DSM

A 1 m by 1 m planimetric grid was generated over the research area. Within each grid cell, the local maximum heights of LiDAR points were distinguished and the maximum height value was stored at each grid location to create a Digital Surface Model (DSM). The DSM was smoothed by a 3x3 Gaussian filter (Hyyppä, et al., 2001) to reduce local variation on the surface. With this 1 m by 1 m smoothed DSM, the slope and aspect were calculated using the function of ArcGIS (ESRI Inc.). The slope and aspect were evaluated by the 3x3 neighboring pixels of DSM (Burrough and McDonnell, 1998).

4.3 Backprojection process

The ground coordinates of grid points from LiDAR derived DSM were transferred to photo-pixel coordinates using the collinearity equations below and an affine transformation. The collinearity equations are:

$$X_a = X_0 - f\left[\frac{m_{11}(X-X_{EX})+m_{12}(Y-Y_{EX})+m_{13}(Z-Z_{EX})}{m_{31}(X-X_{EX})+m_{32}(Y-Y_{EX})+m_{33}(Z-Z_{EX})}\right] \quad (1)$$

$$Y_a = Y_0 - f\left[\frac{m_{21}(X-X_{EX})+m_{22}(Y-Y_{EX})+m_{23}(Z-Z_{EX})}{m_{31}(X-X_{EX})+m_{32}(Y-Y_{EX})+m_{33}(Z-Z_{EX})}\right] \quad (2)$$

(Mikhail et al. 2001)

where m is the rotation matrix based on *omega (ω), phi (φ),* and *kappa* (κ) values of exterior parameters, the subscripts of m_{ij} are the ith row and jth column number of the rotation matrix m. X_a and Y_b are image space coordinates, X_0 and Y_0 are photo centers, f is the focal length, X_{EX}, Y_{EX}, *and* Z_{EX} are the coordinates of perspective centers, and X, Y, *and* Z are the sampled coordinates from LiDAR derived DSM.

To transfer from image space to photo pixel coordinates, an affine transformation (Mikhail et al. 2001) based upon the camera fiducial points was applied.

Note that the resolution of DSM (1 m) and the image pixel resolution of aerial photo (0.15 m) are different. To match the pixel resolution for this fusion technique, the different sizes of spatial filter were applied on the image to find the appropriate size. The following section describes more about the spatial filter.

4.4 Hillshade to cast the shadow on LiDAR derived DSM

With slope and aspect angle derived from the DSM, the shadow was cast using a hillshade function which is a modified version of the equation developed by Burrough and McDonnell (1998). This function is also used for ArcGIS hillshade function of spatial analysis.

$$\text{Hillshade} = 255 * ((\cos(\text{Zenith}) * \cos(\text{Slope})) + (\sin(\text{Zenith}) * \sin(\text{Slope}) * \cos(\text{Azimuth} - \text{Aspect}))) \quad (3)$$

(Burrough and McDonnell, 1998)

where Zenith is 90 – (altitude of the light source), Slope is the surface slope angle derived from the DSM, Azimuth is the azimuth angle of the light source, and Aspect is the surface

aspect derived from the DSM.

The hillshade surface was created in the view of sun and camera location. The hillshade surface used by ArcGIS uses the parallel light ray to calculate Zenith and Azimuth angle over the entire landscape, because the sun altitude is assumed to be at infinity and the azimuth angle is parallel from the sun. However, the camera location mounted on the airborne vehicle has a lower altitude and the azimuth is the radial direction from the camera location. Equation 4 was, therefore, customized to cast the shadow from the camera location in this study.

4.5 Image composition scheme using hillshade function

After respective true orthophotos were created from the three photos, the three true orthophotos were merged to make a composite image. In this study a novel image composition scheme was developed using visible side of hillsahde surface of each acquisition time. The camera view and the sun oriented hillshade surfaces were generated for all images. There were three sun oriented hillshade images and three camera view oriented hillshade images. Each hillshade pixel has the value ranged between 0 and 254. Generally, a hillshade value more than 177 implies the exposed/visible side of the surface towards the sun or camera view and a value less than 177 implies the obscured/occluded side of the surface. These hillshade values among images in the overlapped area were used to compare values and select the higher (or the highest) values to make a composite image from the respective orthophotos.

During the backprojection process, a spatial filter was applied to the filtered region centered at the exact location of drape points on the original perspective photo. This was done because the slight misalignment between draped location from the draped point and exact location should be considered to obtain the color from the original perspective photo. Four different filter sizes were used. The four were the exact location, a 3 by 3 pixels (3x3) filter, a 5 by 5 pixels (5x5) filter, and a 7 by 7 pixels (7x7) filter area (1 pixel cell size is 15 cm). These four cases were used for color acquisition from the original perspective photos.

5. RESULTS

5.1 Aerial Triangulation process of aerial photos

The accuracy from the block triangulation report is shown in Table 2. This shows the variations of GCPs and the location of tie points between each paired image. Table 2 shows the overall RMSE of the block triangulation as 37 cm. The error of comparison with the ground coordinates resulting from the triangulation approach were 37 cm, 48 cm, and 53 cm for the X axis, Y axis, and Z axis respectively.

Ground X coordinate error	37 cm
Ground Y coordinate error	48 cm
Ground Z coordinate error	52 cm
Image X coordinate error	0.13 mm
Image Y coordinate error	0.03 mm
The total RMSE	38 cm

Table 2. The accuracy assessment of aerial triangulation process.

5.2 True orthophoto generation

The improvement of this technique is shown with USGS orthophoto provided by the USGS National Map seamless server. Their orthophoto was captured in the same year (2005) as the aerial photos used in this study. The difference between USGS orthophoto and the true orthophoto was shown on Figure 3. To demonstrate the true projection, the rectified trees in the upright position on the true orthophoto, while trees in the USGS ortho photo were tilted only to show one side.

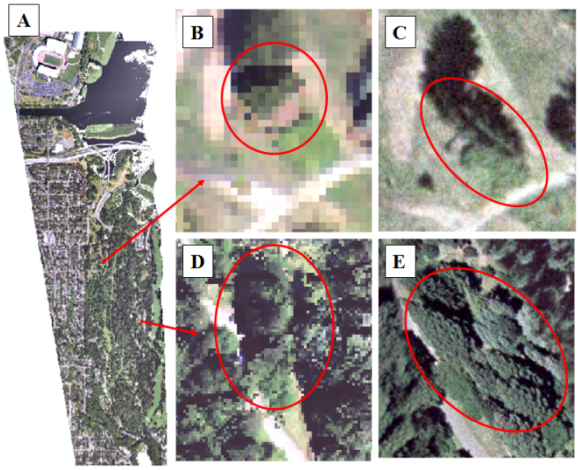

Figure 3. The true orthophoto generation. The final product of true orthophoto for the entire area (A). Single tree shown on the trueortho (B) and the same tree shown on USGS orthophoto (C). A group of trees shown on the trueortho (D) and the same trees shown on USGS orthophoto (E).

5.3 Filter size

Color was obtained for four cases: exact location of draped LiDAR points, a 3x3 filtered region centered at the location of draped LiDAR points on each photo, a 5x5 filtered region, and a 7x7 filtered region. The color variation is smaller and the noise of color values becomes smoother as the size of filter becomes larger. The 7x7 filter is, therefore, appropriate for this case because the color contrast is larger than for the other size of filters. The 7x7 pixel size filer (1 pixel size is 15 cm) is also close to the 1 m by 1 m cell size of LiDAR derived DSM used in this study. A composite image was made from three true orthophotos. Figure 3 shows the resulting composite image with the 7x7 filter and shows the composited true orthophoto for one tree and a group of trees.

6. DISCUSSION

6.1 Accuracy

The RMSE for all axes was less than 50 cm from the block triangulation report that is less error than that reported by St-Onge et al. (2004). The Z coordinates error was larger, because the surveying GPS unit is more error prone in the Z coordinate.

In this study, the conventional way to make an orthophoto was taken using field observed GPS for GCP during aerial triangulation process. GCP can, however, be identified and selected from the LiDAR three dimensional point cloud, if the point density is high enough to visualize objects. Liu et al. (2007) took this approach to derive GCPs from the aerial photos without the actual field survey. They found that LiDAR derived GCPs and DTM from LiDAR significantly reduced positional errors in the orthorectification process. If the GCP location is well identified by LiDAR itself, the error of the mismatch

between field measured GPS and LiDAR elevation acquired by INS can be decreased and the accuracy of the backprojection can be improved. With such an improvement, a smaller filter could be applied to obtain the colors from aerial photos during the composite process and the pixel resolution of DSM could be higher with high density LiDAR points.

With regard to the seasonal difference between the two datasets, the DSM was created with the leaf-off LiDAR data and aerial photos were captured in the leaf-on season. The seasonal difference may have caused some of the noise in the composite image. For example, the noise around trees along the road may be caused by this seasonal difference since the misalignment of the backprojection process was greater. It would be ideal to capture both the LiDAR data and aerial photos at the same time or in the same season.

6.2 Occlusion detection and compensation using hillshade function

As reported by Sheng et al (2003) and Kane et al. (2008), the LiDAR derived DSM does not represent the exact shape of the crown. Especially for parts lower than the lowest branches, the tree shape provided by the DSM is not realistic. To show this effect, Figure 4 shows the hillshade surface using the DSM.

The lower part of the crown had low hillshade values because the hillshade was calculated based on slope and aspect of the surface. If the DSM had abrupt slope change at the sides of tree crown shown on Figure 4, the slope and aspect were never exposed to the camera and sun direction. To show the effect, the edges of tree crowns had black frames which represent the lower values of hillshade in three dimensional view of Figure 4.

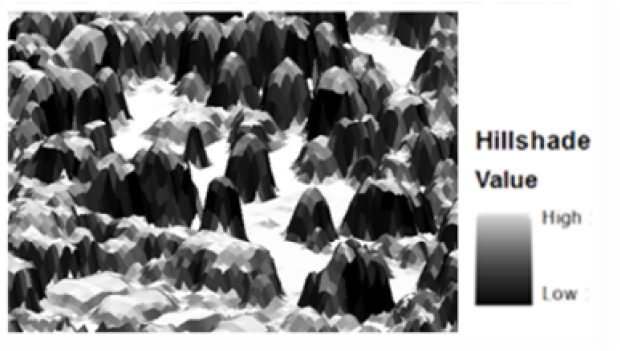

Figure 4. Shadowing effect using hillshade surfaces. Shadows are casted on the side of the DSM, clearly seen from the figure.

The hillshade value is calculated by slope and aspect angles which are evaluated by the gradient of the neighbouring pixels. The abrupt angles at the edge of tree canopy tend to be occluded area. If the tree canopy model is improved to cover the bottom of tree crown, more realistic hillshade values can be calculated and used for the composite process. The wrapped surface (Kato et al., 2009) can provide a more realistic surface to avoid this situation.

Hillshade surfaces provided useful information to find occlusions. If these hillshades are used for the orthorectification process of digital aerial photo with LiDAR taken at the same time, a fully automated true orthophoto process is possible.

6.3 True orthophoto

For the group of trees in Figure 3, the seam (cut) lines appeared on the USGS ortho photo. Conventionally, the final orthophoto tiles were mosaiced from more visually appealing parts of several individually rectified images. These mosaics will exhibit “seam lines” where the individual images met, and tree images at the seam boundaries did not match due to the displacement of tree tops. Even though the aerial photos have been controlled and rectified, the images of trees along the edges of tiles or at seam lines will appear tilted on orthoimages due to perspective angles and the use of DTMs that represent the ground elevations rather than the surface of the tree canopy. This resulted in an orthophoto where ground features were placed in the correct planimetric position, while the treetops were distorted horizontally. Most orthophotos are produced in this manner.

The data fusion using hillshade introduced here can be applied to the data fusion between LiDAR and the other optical spectral datasets at landscape level. The multi- and hyper-spectral images acquired by airborne sensors can have improved rectification with this true orthophoto creation process, even though they are not captured by stereo-pair. The high hillshade values of both camera view and sun angle can be used for spectral calibration. The advantage of this technique is that it selects the pure spectral signature of tree crowns for further species identification with less shadow and shaded pixels, because the exposed side of tree crowns is identified with camera view and sun oriented hillshade surfaces.

7. CONCLUSION

A technique of data fusion between aerial photos and LiDAR was developed. In particular, a true orthophoto was created using the LiDAR derived DSM and hillshade function on the DSM. To make the true orthophoto, backprojection process was used to transfer the ground coordinate to the photo coordinate on the perspective aerial photos using a collinearlity equation. However, to fuse LiDAR derived DSM with aerial photos, only the visible sides of DSM to photo perspectives were required to be identified and selected. The camera view and the sun oriented hillshade surfaces were generated using the LiDAR derived DSM and used to distinguish between the exposed and the occluded side of the DSM. An adapted technique can be applied to the data fusion between LiDAR and multispectral high resolution images, even though the images are not collected with full stereo coverage. If the camera or sensor location is reported, the hillshade function is useful to detect the occluded side of an object to compensate for and correct the color from aerial photos. The pure spectral signature collected with the hillshade surface can also be useful for species identification. Furthermore, the spectral value derived only from the visible side of DSM can be used for color calibration among aerial photos or multi-temporal spectral images. Therefore, this technique dramatically increases the opportunities for the data fusion between LiDAR and any spectral image for the image composition and color calibration.

REFERENCES

Amhar, F., Jansa, J., and Ries, C., Angel, E., 1998. The generation of true orthophotos using a 3D building model in conjunction with a conventional DTM. *International Archive of Photogrammetry and Remote Sensing*, 32 (Part 4): 16-22.

Angel, E., 2003. *Interactive Computer Graphics A Top-Down Approach with OpenGL* (pp. 559-593). NY: Addison Wesley

Brandtberg, T. and Walter F., 1998. Automated delineation of individual tree crowns in high spatial resolution aerial images by multiple-scale analysis. *Machine Vision and Applications* 11, 64-73

Burrough, P. A. and McDonell, R.A., 1998. *Principles of Geographical Information Systems*. New York NY: Oxford University Press

Erikson, M., 2003. Segmentation of individual tree crowns in colour aerial photographs using region growing supported by fuzzy rules. *Canadian Journal of Forest Research* 33, 1557-1563

Gougeon, F.A., 1995. A crown-following approach to the automatic delineation of individual tree crowns in high spatial resolution aerial images. *Canadian Journal of Remote Sensing* 21(3), 274-284

Habib, A.F., Kim E-M., and Kim C-J., 2007. New methodologies for true orthophoto generation. *Photogrammetric Engineering & Remote Sensing*, 73 (1): 25-36.

Hais, M. and Kučera, T., 2008. Surface temperature change of spruce forest as a result of bark beetle attack: remote sensing and GIS approach. *European Journal of Forest Research*, 127:327-336.

Hyyppä, J., Kelle, O., Lehikoinen, M., & Inkinen, M., 2001. A segmentation-based method to retrieve stem volume estimates from 3-D tree height models produced by laser scanners. *IEEE Transactions on Geoscience and Remote Sensing*, 39(5), 969-975

Iverson, L.R., Dale, M.E., Scott, C.T., and Prasad, A., 1997. A GIS-derived integrated moisture index to predict forest composition and productivity of Ohio forests (U.S.A). *Landscape Ecology* 12: 331-348.

Kane, V. R., , Gillespie, A. R., McGaughey, R., James Lutz, J., Ceder, K., and Jerry F. Franklin, J. F., 2008. Interpretation and topographic correction of conifer forest canopy self-shadowing using spectral mixture analysis. *Remote Sensing of Environment* 112(10), 3820-3832.

Kato, A., Moskal, L.M., Schiess, P., Swanson, M.E., Calhoun, D., and Stuetzle, W., 2009. Capturing Tree Crown Formation through Implicit Surface Reconstruction using Airborne Lidar Data, *Remote Sensing of Environment* 113: pp1148-1162

Leckie, D., Gougeon, F., Hill, D., Quinn, E.,Armstrong, L., and Shreenan, R., 2003. Combined high-density lidar and multispectral imagery for individual tree crown analysis. *Canadian Journal of Remote Sensing* 29(5), 633-649

Leckie, D.G., Gougeon, F.A., Tinis, S., Nelson, T., Burnett, C. N., and Paradine, D., 2005. Automated tree recognition in old growth conifer stands with high resolution digital imagery. *Remote Sensing of Environment* 94, 311-326

Liu, X., Zhang, Z., Peterson, J., and Chandra, S., 2007. LiDAR-derived high quality ground control information and DEM for Image Orthorectification. *Geoinformatica* 11, 37-53

Mahiny, A.S. and Gholamalifard, M., 2007. Dynamic spatial modeling of urban growth through cellular automata in a GIS environment. *International Journal of Environment Research* 1(3): 272-279.

Mikhail, E.M., Bethel, J.S., and McGlone, J.C., 2001. *Introduction to modern photogrammetry* New York, NY: John Wiley & Sons, Inc.

Pellegrini, L., Boni, P., and Carton, A., 2003. Hydrographic evolution in relation to neotectonics aided by data processing and assessment: some examples from the Northen Apennines (Italy). *Quaternary International* 101-102: 211-217.

Rau, J-Y., Chen, N-Y, and Chen L-C., 2002. True orthophoto generation of built-up areas using multi-view images. *Photogrammetric Engineering and Remote Sensing* 68 (6): 581-588.

Rönnholm, P., Hyyppä, J.,Hyyppä, H.,Haggrén, H., Yu, X., and Kaartinen, H., 2004. Calibration of laser-derived tree height estimates by means of photogrammetric techniques. *Scandinavian Journal of Forest Research* 19, 524-528

Schickler W. and Thorpe A., 1998. Operational procedure for automatic true orthophoto generation. *International Archive of Photogrammetry and Remote Sensing* 32 (Part 4): 527-532.

Sheng Y., Gong, P. and Biging, G.S., 2003. True orthoimage production for forested areas from large-scale aerial photographs. *Photogrammetric Engineering and Remote Sensing* 69 (3): 259-266.

St-Onge, B., Jumelet, J., Cobello, M., and Véga, C., 2004. Measuring individual tree height using a combination of stereophotogrammetry and lidar. *Canadian Journal of Remote Sensing* 34, 2122-2130

Van Den Eeckhaut, M, Poesen, J., Verstraeten, G., Vaanacker, V., Moeyersons, J., Nyssen, J., and van Beek, L.P.H., 2005. The effectiveness of hilldshade maps and expert knowledge in mapping old deep-seated landslides. *Geomorphology* 67: 351-363.

Van Den Eeckhaut, M., Poesen, J., Verstraeten, G. Vaanacker, V., Nyssen, J., Moeyersons, J., van Beek, L.P.H, and Vandekerckhove, L., 2007. Use of LIDAR-derived images for mapping old slides under forest, *Earth Surface Processes and Landforms* 32: 754-769.

Wulder, M., Niemann, K.O., and Goodenough, D.G., 2000. Local maximum filtering for the extraction of tree locations and basal area from high spatial resolution imagery. *Remote Sensing of Environment* 73, 103-114

Zhou, G., Chen, W., Kelmelis, J.A., and Zhang, D., 2005. A comprehensive study on urban true orthorectification. *IEEE Transactions on Geoscience and Remote Sensing* 43 (9): 2138-2147.

ACKNOWLEDGEMENTS

The authors would like to express our sincere gratitude to Dr. Ward W. Carson of the former USDA Forest Services and American Society of Photogrammetry and Remote Sensing for giving two awards (2008 Ta Liang Award and 2008 Paul R. Wolf Scholarship) to support this research.